Preserving polarimetric properties in PolSAR image reconstruction through Complex-Valued Auto-Encoders

Quentin Gabot, Jérémy Fix, Joana Frontera-Pons, Chengfang Ren, Jean-Philippe Ovarlez

Preserving polarimetric properties in PolSAR image reconstruction through Complex-Valued Auto-Encoders

Quentin Gabot*‡, Jérémy Fix†, Joana Frontera-Pons‡ Chengfang Ren* and Jean-Philippe Ovarlez*‡
*SONDRA, CentraleSupélec, Université Paris-Saclay, 91190 Gif-sur-Yvette, France,
†LORIA, CNRS, CentraleSupélec, Université Paris-Saclay, F-57000 Metz, France,
‡DEMR, ONERA, Université Paris Saclay, F-91123 Palaiseau, France,

***Abstract*—The complex-valued nature of Polarimetric SAR data requires dedicated algorithms that can deal with complex-valued representations. This approach needs to be studied more in the deep learning community, where several works instead transformed the complex-valued signals into the real domain before applying standard real-valued algorithms. In this paper, we employ complex-valued neural networks and study the performance of complex-valued convolutional autoencoders. We demonstrate the ability of such networks to compress fully polarimetric SAR data and decompress them by preserving critical physical properties as revealed by the Pauli and Krogager coherent decompositions and the non-coherent $H - \alpha$ decomposition.**

***Index Terms*—Complex-valued Auto-Encoders, PolSAR image reconstruction, polarimetric decompositions**

I. Introduction

Synthetic Aperture Radar (SAR) polarimetry is a widely used technique for the derivation of qualitative and quantitative physical information for land, snow and ice, ocean, and urban applications based on the measurement and exploration of the polarimetric properties of artificial and natural scatterers [1]. Just like every SAR imaging technique (interferometry, tomography, etc.), SAR polarimetry provides high-resolution, day-and-night and weather-independent images for a multitude of applications ranging from geoscience and climate change research, environmental and Earth system monitoring [2]. Thus, PolSAR imaging differs drastically from the omnipresent optical imaging in the computer vision field. Whether due to the notion of speckle or the complex-valued nature of PolSAR images, the traditional techniques used in the computer vision field can not be applied.

To tackle this limitation, the scientific community often sacrificed the phase information in favor of the sole amplitude information to transform SAR images into single channel real-valued ones on which to apply well-studied real-valued neural networks [3], which happen to be much closer to the traditional optical images than SAR images. Nevertheless, the phase information is critical for advanced techniques like SAR polarimetry or SAR interferometry, and the machine learning algorithms should not drop it.

Several works already studied complex-valued neural networks [4]–[6], demonstrating their unique properties to real-valued neural networks. Of particular interest for our work is [7], who studied complex-valued autoencoders and, in the field of SAR, the works of [8], [9] studied complex-valued AutoEncoders applied to sentinel-1 data with dual-polarizations for a classification task.

In this paper, we push forward the study of the performances of complex-valued AutoEncoders applied to SAR data by demonstrating their ability to preserve polarimetric properties in fully polarimetric SAR image reconstruction. The paper is structured as follows: we first present some fundamental polarimetric properties inherent to PolSAR images in Section II-A that we seek to preserve. Then, we discuss the reconstruction process itself by presenting the complex-valued variant of the Convolutional Auto-Encoder model that we use in Section II-D. Finally, we present the encouraging results obtained throughout multiple experiments in Section III. This work is the first milestone in proposing a generative modeling process trained on PolSAR images.

II. Methodology

A. Polarimetric SAR decompositions

SAR Polarimetry exploits the polarization properties of electromagnetic waves to measure the polarimetric properties of scatterers. This technique derives qualitative and quantitative physical information related to ground physics (building, vehicles, forest, sea, road, crops, etc.). Thus, each pixel of the image is associated with a complex scattering matrix S, called the Sinclair matrix:

$$S = \begin{pmatrix} S_{HH} & S_{VH} \\ S_{HV} & S_{VV} \end{pmatrix} \tag{1}$$

The indices H and V refer to the horizontal and vertical polarization states, but any orthogonal polarimetry basis can be used. In the context of monostatic SAR, this matrix is symmetric, *i.e.* $S_{HV} = S_{VH}$. [10]. Then, a full PolSAR image is a complex-valued tensor $\in \mathbb{C}^{3\times h\times w}$ where h and w are the image height and width respectively.

B. Coherent Polarimetric Decomposition

The usual tool for studying the Sinclair matrix is based on coherent decompositions, which involve expressing $\mathbf{S}$ as a combination of the backscattering mechanism response of canonical objects. The underlying reason is that significant dispersion and anisotropy phenomena are expected from coherent

(or artificial) targets (e.g., cars, airplanes, trucks, buildings, etc.), unlike non-deterministic targets such as vegetation (e.g., crops, forests, etc.). Therefore, these decompositions can help us to distinguish them better. Two well-known representations are usually used: the Pauli and the Krogager decomposition.

1) Pauli decomposition: In the context of monostatic SAR, the Pauli decomposition [11] expresses $\mathbf{S}$ as:

$$\mathbf{S} = \frac{\alpha}{2}\begin{pmatrix}1 & 0\\ 0 & 1\end{pmatrix} + \frac{\beta}{2}\begin{pmatrix}1 & 0\\ 0 & -1\end{pmatrix} + \frac{\gamma}{2}\begin{pmatrix}0 & 1\\ 1 & 0\end{pmatrix}, \qquad (2)$$

where each term $\alpha = S_{HH} + S_{VV}$, $\beta = S_{HH} - S_{VV}$ and $\gamma = 2S_{HV}$ represent the part of the response of a plate observed at normal incidence or a sphere, the characteristic of a horizontal metallic dihedral and the scattering matrix of a metallic dihedral oriented at $45°$ with respect to the radar line of sight respectively. Then, we define the Pauli vector as $\mathbf{k} = \frac{1}{\sqrt{2}}(\alpha \;\; \beta \;\; \gamma)^T$ which is usually used to estimate the coherence matrix in eq. (5) and to plot an RGB image by taking the module of each component.

2) Krogager Decomposition: A refined alternative approach, proposed by [12]–[14] considers a scattering matrix as the combination of the responses of a sphere, an oriented diplane and a helix:

$$\mathbf{S} = e^{j\varphi}\left(e^{j\varphi_s}\, k_s\, \mathbf{S}_s + k_d\, \mathbf{S}_d(\vartheta) + k_h\, \mathbf{S}_h(\vartheta)\right), \qquad (3)$$

where $\mathbf{S}_s = \begin{pmatrix}1 & 0\\ 0 & 1\end{pmatrix}$, $\mathbf{S}_d(\vartheta) = \begin{pmatrix}\cos 2\vartheta & \sin 2\vartheta\\ \sin 2\vartheta & -\cos 2\vartheta\end{pmatrix}$ and $\mathbf{S}_h(\vartheta) = e^{\pm 2j\vartheta}\begin{pmatrix}1 & \pm j\\ \pm j & -1\end{pmatrix}$, where the $\pm$ sign in the helix component varies the left or right handedness, and has to be fixed during the estimation of its components. The identification of the parameters is generally performed in the right-left circular basis:

$$\begin{cases} k_s = |S_{RL}|, \\ k_h = |S_{RR}| - |S_{LL}|,\ k_d = |S_{LL}| & \text{if } |S_{RR}| > |S_{LL}| \\ k_h = |S_{LL}| - |S_{RR}|,\ k_d = |S_{RR}| & \text{otherwise} \end{cases} \qquad (4)$$

The condition $|S_{RR}| > |S_{LL}|$ denotes the presence of a left-handed helix contribution. The coefficients k_s, k_d, and k_h represent the amplitude of each canonical scattering mechanism contributing to the initially measured scattering matrix $\mathbf{S}$.

From the Krogager decomposition, we can deduce the vector $\mathbf{h} = (k_d \;\; k_h \;\; k_s)^T$ which is usually used to plot a RGB image.

C. Non-Coherent Polarimetric Decomposition

Although coherent decompositions help describe artificial targets, they are not suited to analyze random scattering effects (forests, fields, vegetation, etc.). To fill this lack, the Pauli vector $\mathbf{k}$ is usually modeled by the multivariate, centered, circular complex Gaussian distribution $\mathcal{CN}(\mathbf{0}, \mathbf{T})$ which is fully characterized by the covariance matrix $\mathbf{T} = E\left[\mathbf{k}\,\mathbf{k}^H\right]$. This covariance matrix is estimated locally on a PolSAR image

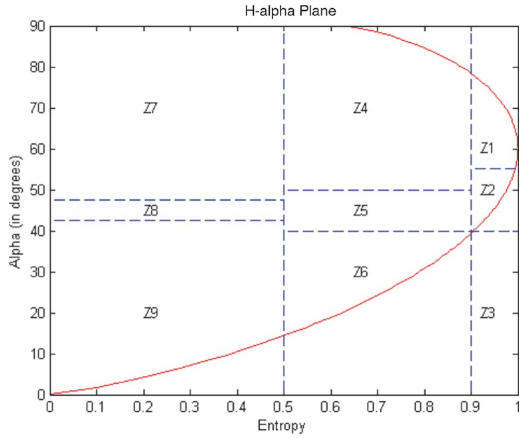

Fig. 1: $H - \alpha$ plane separated into areas Z1 to Z9, each one corresponding to a specific scattering mechanism. The red line represents the boundary of physically possible $H - \alpha$ couples.

through the Sample Covariance Matrix (SCM) $\hat{\mathbf{T}}$ computed on a set of N samples taken in a spatial boxcar:

$$\hat{\mathbf{T}} = \frac{1}{N}\sum_{i=1}^{N} \mathbf{k}_i\, \mathbf{k}_i^H. \qquad (5)$$

The entropy, H, indicates the randomness of the overall backscattering phenomenon: $H = \sum_{i=1}^{3} p_i \log p_i$ with the pseudo-probabilities $p_i = \lambda_i / \left(\sum_{j=1}^{3} \lambda_j\right)$ and λ_i the eigenvalues of the covariance matrix. Entropy varies between 0 and 1. A low entropy indicates that the observed target is pure and the backscattering is deterministic. This is reflected by a single non-zero normalized eigenvalue close to 1. When the entropy is high, it reflects the completely random nature of the observed target. This occurs when the pseudo-probabilities are identical.

The angle $\alpha = \sum_{i=1}^{3} p_i \alpha_i$ with $\alpha_i = \arccos(|e_{i1}|)$ and e_{i1} the first component of the i-th eigenvector of the SCM. It varies between $0°$ and $90°$ and characterizes the type of the dominant scattering mechanism (surface diffusion, dihedral diffusion). The relationship between entropy, α angle and scattering mechanisms is represented in Figure 1. Based on the entropy and alpha parameters, a classification procedure can be envisioned. Indeed, by considering the two-dimensional $H - \alpha$ space, all random scattering mechanisms can be represented [15]. Therefore, a pixel's belonging to a region of the $H - \alpha$ plane allows for a physical interpretation of the average scattering mechanism involved.

D. Complex-valued AutoEncoders

As explained in [16], an AutoEncoder (AE) is a neural network that encodes the input in a latent space and reconstruct its input signal via a decoder. Consequently, when dealing with spatial data types like images, the encoding and decoding are done using convolution layers: such models are called Convolutional Autoencoders (CoAEs or CAEs) [17]. In this work, we extended the CAE architecture to complex-valued data, similarly to [18], [19]. The AE structure usually includes

three parts (with the latent space being implicitly defined in some cases):

- Encoder: compression of the input data X by progressively reducing its dimensionality. In the case of a CoAE, the encoder is a succession of convolutional layers, activation functions and spatial downsampling,
- Latent space: the bottleneck between the encoder and the decoder. It may be explicitly expressed in the form of a flattened dense layer of dimension p,
- Decoder: it turns the converted data back to the original space by restoring its initial dimensionality, resulting in a reconstructed data $\hat{\mathbf{X}}$. In the case of a CoAE, the decoder is a succession of spatial upsampling, convolutional layers and activation functions.

The AE (and by extension the CoAE) is trained under the unsupervised learning paradigm to find the set of parameters θ that minimizes the reconstruction error between $\mathbf{X}$ and $\hat{\mathbf{X}}$: the loss function is usually taken to be the Mean Squared Error (MSE). Learning a good representation of PolSAR images is difficult task due to the complex-valued nature and polarimetric channels. Indeed, preserving both information after the reconstruction process is essential as PolSAR images are made of complex-valued Sinclair vectors representing scatterers' amplitude and phase information in a scene. As explained in Section II-A, the amplitude and phase of the backscattered signal depend on the physical and electrical properties of the imaged scene; thus, a proper representation for PolSAR images is synonymous with being able to preserve the amplitude and phase information after the encoding and decoding process of the model. Standard deep learning models are considered and designed with the real-valued case in mind; such models are categorized under the appellation Real-Valued Neural Networks (RVNNs).Multiple ways of handling this problem have been proposed.

Many approaches need to pay more attention to the phase information and work on the amplitude information, as seen in this recent survey on deep generative modeling for SAR images [20]. The complex-valued data are transformed into real-valued data, and the usual RVNN models are used. To keep the phase information, a straightforward approach is to consider that complex-valued representations can be expressed as stacked real-valued representations.

Complex-Valued Neural Networks (CVNNs) were first thought to be equivalent to two-dimensional RVNNs, also known as split-CVNNs [21], [22]. Nevertheless, as pointed out by A. Hirose [5], split-CVNNs are easy to implement and comprehend as they are essentially RVNNs but not equivalent to CVNNs. The main difference between them is the multiplication operation: indeed, a complex-valued multiplication is essentially the composition of a rotation and a homothety in the complex plane, which would have more parameters for its real-valued counterpart [23], [24]. Additionally, as pointed out in [25], CVNNs outperform RVNNs (and thus split-CVNNs) when dealing with phase-sensitive tasks. Nevertheless, it is essential to recognize that CVNNs learn slower than RVNNs [25]. With complex-valued neural networks, there is still room for research to find the most appropriate loss and activation functions benefiting from the specificities of the complex nature of the representation.

In our work, we implement a complex-valued Auto-Encoder (CoAE). As explained in Section II-A, PolSAR images are complex-valued tensors of dimension $(3, h, w)$ to be passed as input to the complex-valued CoAE. More specifically, let us denote the encoder $E : \mathbb{C}^{3\times h\times w} \rightarrow \mathbb{C}^p$ and the decoder $D : \mathbb{C}^p \rightarrow \mathbb{C}^{3\times h\times w}$ with p being the size of the latent space, such as illustrated in Figure 2.

The activation functions are placed between the consecutive convolutional layers (as well as the transposed convolutional layers). The numerous complex-valued activation functions proposed by the scientific community [22] are designed to be non-linear and avoid the exploding/vanishing gradient problem during training. In the context of CVNNs, these activation functions can be fully-complex such as the $\tanh$ [21] or can be classified as either Type A, when the function is applied separately on the real & imaginary parts such as the $\mathbb{C}$ReLU or Type B when applied only on the magnitude while preserving phase such as the $\mathrm{modReLU}(z)$ function: $\mathrm{modReLU}(z) = \mathrm{ReLU}(r+\beta)e^{j\theta} = \begin{cases} (r+\beta)e^{j\theta} & \text{if } (r+\beta) \geq 0, \\ 0 & \text{otherwise.} \end{cases}$ [22]. In this research study, we have opted for using the $\mathrm{modReLU}$ activation function due to observations from some early experiments of its ability to reduce the time required for the model to converge drastically.

Concerning the loss function $L : \mathbb{C}^t \times \mathbb{C}^t \longrightarrow \mathbb{R}$, the output domain has to be real-valued for the minimization of the loss, and its input domain $\mathbb{C}^t$ should support complex-valued input, e.g., complex-valued weights and convolutional kernels. In the context of AE, the loss function we consider is the standard MSE extended to the complex domain: $\mathrm{L}\left(\hat{\mathbf{X}}, \mathbf{X}\right) = \frac{1}{n}\sum_{i=1}^{n}\left|\hat{\mathbf{X}}_i - \mathbf{X}_i\right|^2$ [26], [27]. One last segment of our complex-valued CoAE needs to be addressed: the back-propagation. Implementing a complex-valued backpropagation has been a theoretical problem due to the implications of Liouville theorem [28]. Indeed, while the backpropagation algorithm relies upon the computation of a succession of partial derivatives, using non-holomorphic functions leads to an incompatibility to compute the complex derivative. However, the introduction of Wirtinger calculus [29] allows the generalization of the complex derivative to non-holomorphic functions, leading to the following definition of the gradient: $\nabla_z f = 2\frac{\partial f}{\partial \overline{z}} = \frac{\partial f}{\partial x} + i\frac{\partial f}{\partial y}$. Afterward, the back-propagation and the computational graph are extended to the complex domain [30]. All the experiments in this paper are performed using Pytorch [31], which provides, in particular, the implementation of Wirtinger calculus. The code for the experiments is provided online at https://t.ly/biiId.

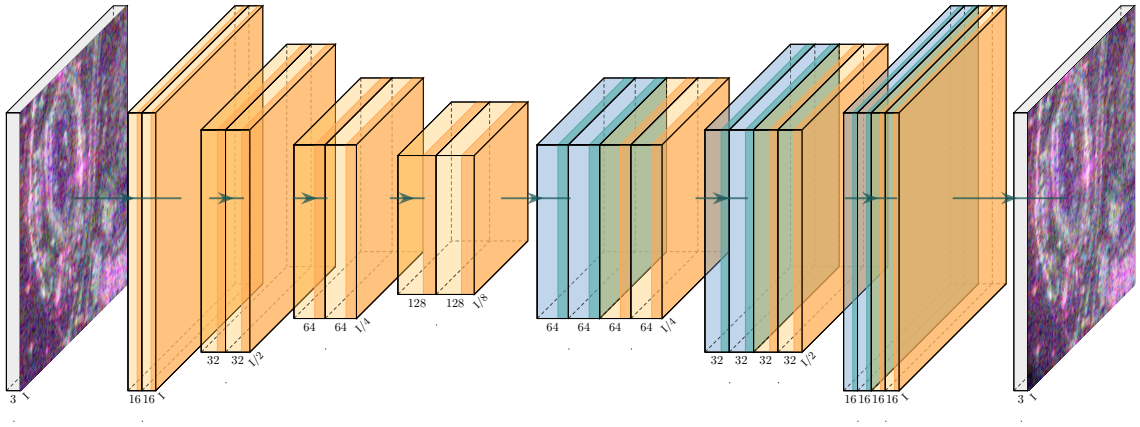

Fig. 2: Architecture of a CoAE where yellow layers represent complex-valued convolutional layers while blue layers represent complex-valued transposed convolutional layers.

III. Results

To validate our approach, we have tested our method on the San Francisco Polarimetric SAR ALOS-2 dataset[1]. This L-band polarimetric SAR image with a ground range resolution approximating 10m has been acquired by the satellite ALOS-2: due to the penetration capability of L-band wave into forest, vegetation, snow, and soil medium, ALOS-2 brought precious information on the earth surface objects [32].

The dataset is built by cropping the 22608×8080 image into 64×64 non overlapping tiles. The tiles are randomly assigned to the training and validation folds with 80% for training and 20% for validation. Concerning the training of our complex-valued CoAE, we have opted for the AdamW optimizer [33] with a weight decay of $5e^{-4}$ and a learning rate of $1e^{-4}$. The model is trained during 1500 with an early stopping strategy: in our case, the loss converged after 600 epochs, displaying negligible variation afterward, as illustrated in Figure 3.

After training the complex-valued CoAE, we can reassemble the reconstructed crops and compare the reconstructed image to the original one. For instance, as our approach is based on complex-valued data, we can calculate the pixel-wise error for both the phase and amplitude. These error histograms, computed on the validation fold, are shown in Figure 4.

This highlights the excellent capacity of our model to reconstruct the original image faithfully at a pixel-wise level.

Looking at a more global level, we can see that our model also successfully reconstructs an image with very similar polarimetric properties to the original. Indeed, we can display both images using the Pauli basis, as illustrated in Figure 5, and the Krogager basis, as illustrated in Figure 6. With these coherent polarimetric decompositions, we can observe that the polarimetric properties are well preserved.

[1]https://ietr-lab.univ-rennes1.fr/polsarpro-bio/san-francisco/

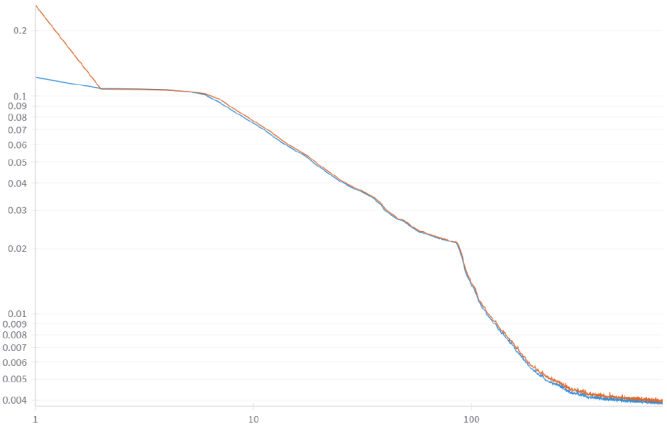

Fig. 3: Complex-valued MSE loss for the train (blue) and valid (orange) set in log-log scale. This MSE is computed on the Sinclair matrix.

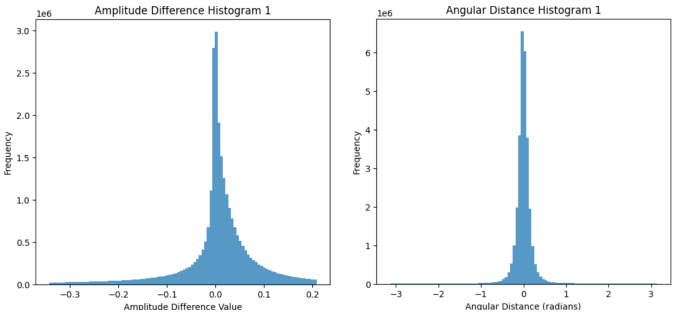

Fig. 4: Amplitude and phase differences between original and reconstructed image computed on the validation fold.

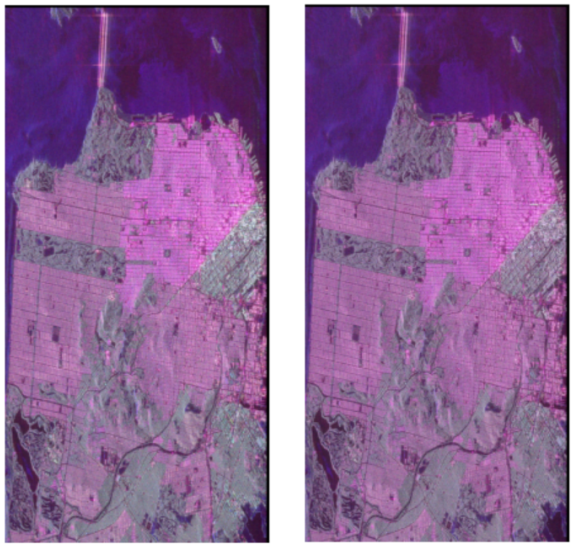

Fig. 5: Amplitude images of the original (left) and reconstructed (right) images with the Pauli basis

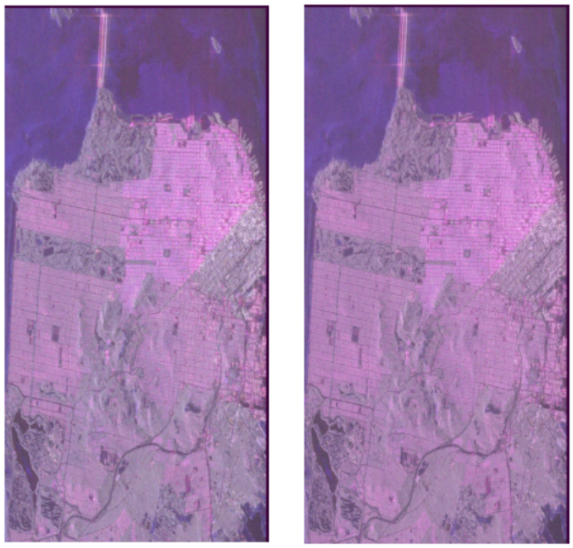

Fig. 6: Amplitude images of the original (left) and reconstructed (right) images with the Krogager basis

Finally, we can see that the properties are also preserved when looking at the $H - \alpha$ non-coherent decomposition, as illustrated in Figure 7. This representation is interesting as it equally shows the impressive preservation capacities of the complex-valued CoAE and highlights some of its limitations. Indeed, when referring to the confusion matrix in Figure 8, we can observe the overall good preservation of the labels throughout the reconstruction process. The accuracy is 73.91%, which leaves some room for improvement. With the help of Figure 1, we can see that the misclassifications occur with neighboring regions of the $H - \alpha$ plane, which have similar scattering properties. Although the mean squared error favors the reconstruction of the energy, hence favors the reconstruction of the $H - \alpha$, the model is unaware of the boundaries of the $H - \alpha$ regions during its training. There is, therefore, nothing in this loss that prevents pixels from crossing the borders. It may seem that only minimizing the mean squared error might not be a sufficient criterion to preserve more subtle polarimetric properties, such as the $H-\alpha$ classification.

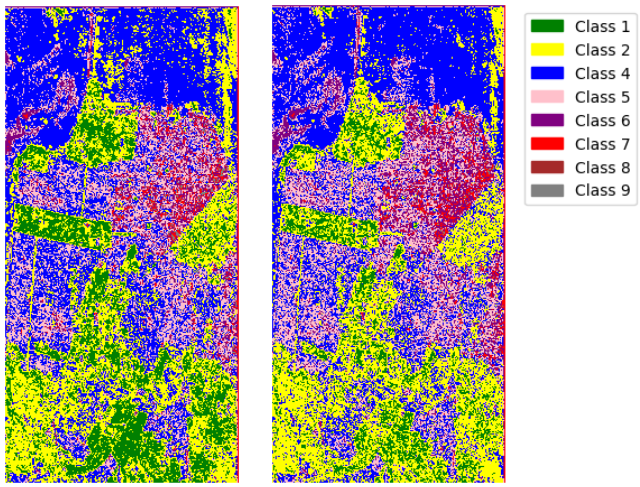

Fig. 7: Images of the original (left) and reconstructed (right) images with the $H - \alpha$ classification

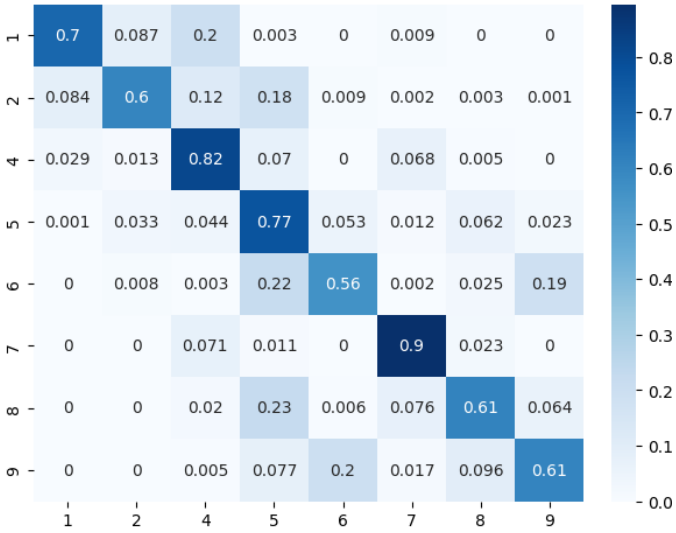

Fig. 8: Confusion matrix of the original (rows) and reconstructed (columns) $H - \alpha$ classes

IV. Discussion

In recent years, combining techniques from the artificial intelligence field, specifically deep learning, such as deep generative modeling, into non-optical computer vision domains like SAR imaging has become a challenge. Indeed, due to

the numerous particularities of SAR imaging, as well as the existence of advanced techniques such as polarimetric SAR, adapting standard methods from the field of deep learning computer vision is a challenging task. In this work, we have demonstrated the capacity of a complex-valued Convolutional Auto-Encoder to preserve fundamental polarimetric properties throughout a reconstruction process. In other words, a latent vector representing a PolSAR image can be decoded while still retaining most of its physical properties. We have used coherent decompositions, such as Pauli and Krogager decompositions, and non-coherent decompositions, such as $H - \alpha$ decomposition, to validate this hypothesis. The preservation is impressive in both cases, considering that the mean squared error is the only criterion minimized during the model training. Nevertheless, the 73.91% global accuracy of the $H - \alpha$ classification reconstruction highlights that these physical properties might have to be integrated into the training process to achieve almost perfect preservation of physical properties during the reconstruction (and, by extension, generation) process. This result may pave the way for many more research works, such as generating coherent synthetic PolSAR images.

REFERENCES

[1] F. M. Henderson and A. J. Lewis, *Manual of remote sensing: principles and applications of imaging radar*, Wiley, 1998.

[2] F. M. Henderson and Z.-G. Xia, "SAR applications in human settlement detection, population estimation and urban land use pattern analysis: a status report," *IEEE transactions on geoscience and remote sensing*, vol. 35, no. 1, pp. 79–85, 1997.

[3] J. Frontera-Pons, F. Brigui, and X. De Milly, "Unsupervised SAR change detection with despeckling autoencoders," in *2023 IEEE International Radar Conference (RADAR)*. IEEE, 2023, pp. 1–6.

[4] A. Hirose, "Complex-valued neural networks: The merits and their origins," in *2009 International Joint Conference on Neural Networks*, Atlanta, Ga, USA, June 2009, pp. 1237–1244, IEEE.

[5] A. Hirose and S. Yoshida, "Generalization Characteristics of Complex-Valued Feedforward Neural Networks in Relation to Signal Coherence," *IEEE Transactions on Neural Networks and Learning Systems*, vol. 23, no. 4, pp. 541–551, Apr. 2012.

[6] J. A. Barrachina, C. Ren, C. Morisseau, G. Vieillard, and J.-P. Ovarlez, "Complex-valued vs. real-valued neural networks for classification perspectives: An example on non-circular data," in *ICASSP 2021 - 2021 IEEE International Conference on Acoustics, Speech and Signal Processing (ICASSP)*, 2021, pp. 2990–2994.

[7] R. Shang, G. Wang, A. Okoth, and L. Jiao, "Complex-Valued Convolutional Autoencoder and Spatial Pixel-Squares Refinement for Polarimetric SAR Image Classification," *Remote Sensing*, vol. 11, no. 5, pp. 522, Mar. 2019.

[8] R. Mohammadi Asiyabi, M. Datcu, A. Anghel, and H. Nies, "Complex-valued end-to-end deep network with coherency preservation for complex-valued SAR data reconstruction and classification," *IEEE Transactions on Geoscience and Remote Sensing*, vol. 61, pp. 1–17, 2023.

[9] R. Mohammadi Asiyabi, M. Datcu, A. Anghel, and H. Nies, "Complex-valued autoencoders with coherence preservation for SAR," in *EUSAR 2022; 14th European Conference on Synthetic Aperture Radar*, 2022, pp. 1–6.

[10] S. Quegan, *Understanding synthetic aperture radar images*, The SciTech radar und defense series. SciTech Publishing, Inc, Raleigh, NC, 2004.

[11] V. Alberga, E. Krogager, M. Chandra, and G. Wanielik, "Potential of coherent decompositions in SAR polarimetry and interferometry," in *IGARSS 2004. 2004 IEEE International Geoscience and Remote Sensing Symposium*, 2004, vol. 3, pp. 1792–1795 vol.3.

[12] E. Krogager, "Utilization and interpretation of polarimetric data in high resolution radar target imaging," in *Proc. Second International Workshop on Radar Polarimetry (JIPR'1992)*, Nantes, France, Sept. 8–10, 1992, vol. 2, pp. 547–557.

[13] E. Krogager and Z. H. Czyz, "Properties of the sphere, diplane, helix decomposition," in *Proc. Third International Workshop on Radar Polarimetry (JIPR'1995)*, Nantes, France, Mar. 21–23, 1995, vol. 1, pp. 106–114.

[14] E. Krogager, J. Dall, and S. N. Madsen, "The sphere, diplane, helix decomposition recent results with polarimetric SAR data," in *Proc. Third International Workshop on Radar Polarimetry (JIPR'1995)*, Nantes, France, Mar. 21–23, 1995, vol. 2, pp. 621–625.

[15] P. Formont, F. Pascal, G. Vasile, J.-P. Ovarlez, and L. Ferro-Famil, "Statistical classification for heterogeneous polarimetric SAR images," *IEEE Journal of selected topics in Signal Processing*, vol. 5, no. 3, pp. 567–576, 2010.

[16] D. E. Rumelhart, G. E. Hinton, and R. J. Williams, "Learning representations by back-propagating errors," *Nature*, vol. 323, no. 6088, pp. 533–536, Oct. 1986.

[17] J. Masci, U. Meier, D. Cireşan, and J. Schmidhuber, "Stacked Convolutional Auto-Encoders for Hierarchical Feature Extraction," in *Artificial Neural Networks and Machine Learning – ICANN 2011*, T. Honkela, W. Duch, M. Girolami, and S. Kaski, Eds., vol. 6791, pp. 52–59. Springer Berlin Heidelberg, Berlin, Heidelberg, 2011, Series Title: Lecture Notes in Computer Science.

[18] S. Löwe, P. Lippe, M. Rudolph, and M. Welling, "Complex-valued autoencoders for object discovery," *arXiv preprint arXiv:2204.02075*, 2022.

[19] P. Baldi and Z. Lu, "Complex-valued autoencoders," *Neural Networks*, vol. 33, pp. 136–147, 2012.

[20] J. Zhang, Z. Liu, W. Jiang, Y. Liu, X. Zhou, and X. Li, "Application of deep generative networks for SAR/ISAR: a review," *Artificial Intelligence Review*, vol. 56, no. 10, pp. 11905–11983, Oct. 2023.

[21] C. Lee, H. Hasegawa, and S. Gao, "Complex-Valued Neural Networks: A Comprehensive Survey," *IEEE/CAA Journal of Automatica Sinica*, vol. 9, no. 8, pp. 1406–1426, Aug. 2022.

[22] J. Bassey, L. Qian, and X. Li, "A Survey of Complex-Valued Neural Networks," Jan. 2021, arxiv: 2101.12249v1.

[23] J. A. Barrachina, C. Ren, C. Morisseau, G. Vieillard, and J.-P. Ovarlez, "Comparison Between Equivalent Architectures of Complex-valued and Real-valued Neural Networks - Application on Polarimetric SAR Image Segmentation," *Journal of Signal Processing Systems*, July 2022.

[24] J. A. Barrachina, C. Ren, G. Vieillard, C. Morisseau, and J.-P. Ovarlez, "Real- and complex-valued neural networks for SAR image segmentation through different polarimetric representations," in *2022 IEEE International Conference on Image Processing (ICIP)*, 2022, pp. 1456–1460.

[25] J.-H. Wu, S.-Q. Zhang, Y. Jiang, and Z.-H. Zhou, "Complex-valued Neurons Can Learn More but Slower than Real-valued Neurons via Gradient Descent," in *Thirty-seventh Conference on Neural Information Processing Systems*, 2023.

[26] R. Hänsch, "Complex-Valued Multi-Layer Perceptrons – An Application to Polarimetric SAR Data," *Photogrammetric Engineering & Remote Sensing*, vol. 76, no. 9, pp. 1081–1088, Sept. 2010.

[27] A. Prashanth, P. K. Kalra, and N. S. Vyas, "Surface classification using ANN and complex-valued neural network," in *Proceedings of the 9th International Conference on Neural Information Processing, 2002. ICONIP '02.*, Singapore, 2002, pp. 1094–1098, Nanyang Technol. Univ.

[28] A. Hirose, Ed., *Complex-Valued Neural Networks: Advances and Applications*, Wiley, 1 edition, Apr. 2013.

[29] W. Wirtinger, "Zur formalen theorie der funktionen von mehr komplexen veränderlichen," *Mathematische Annalen*, vol. 97, pp. 357–375, 1927.

[30] K. Kreutz-Delgado, "The complex gradient operator and the CR-calculus," *arXiv preprint arXiv:0906.4835*, 2009.

[31] A. Paszke, S. Gross, F. Massa, A. Lerer, J. Bradbury, G. Chanan, T. Killeen, Z. Lin, N. Gimelshein, L. Antiga, A. Desmaison, A. Köpf, E. Yang, Z. DeVito, M. Raison, A. Tejani, S. Chilamkurthy, B. Steiner, L. Fang, J. Bai, and S. Chintala, "Pytorch: an imperative style, high-performance deep learning library," in *Proceedings of the 33rd International Conference on Neural Information Processing Systems*, Red Hook, NY, USA, 2019, Curran Associates Inc.

[32] Y. Yamaguchi, R. Sato, and H. Yamada, "ALOS-2 quad. pol. images and ALOS ones," in *Proceedings of EUSAR 2016: 11th European Conference on Synthetic Aperture Radar*, 2016, pp. 1–4.

[33] I. Loshchilov and F. Hutter, "Decoupled weight decay regularization," *arXiv preprint arXiv:1711.05101*, 2017.